Published in final edited form as:
Chem Res Toxicol. 2012 August 20; 25(8): 1643–1651. doi:10.1021/tx3001048.

Metabolic Impact of 4-Hydroxynonenal on Macrophage-Like RAW 264.7 Function and Activation

Reese S. Harry, **Leslie A. Hiatt**, **Danielle W. Kimmel**, **Clare K. Carney**, **Kristin C. Halfpenny**, **David E. Cliffel**[*], and **David W. Wright**[*]
All authors associated with the Department of Chemistry, Vanderbilt University, 7330 Stevenson Center, VU Station B 351822, Nashville, TN 3723501822, USA.

Abstract

Metabolic profiling of macrophage metabolic response upon exposure to 4-hydroxynonenal (HNE) demonstrates that HNE does not simply inactivate superoxide generating enzymes but could also be responsible for the impairment of downfield signaling pathways. Multianalyte microphysiometry (MAMP) was employed to simultaneously measure perturbations in extracellular acidification, lactate production and oxygen consumption for the examination of aerobic and anaerobic pathways. Combining the activation of oxidative burst with phorbol myristate acetate (PMA) and the immunosuppression with HNE, the complex nature of HNE toxicity was determined to be concentration- and time-dependent. Further analysis was utilized to assess the temporal effect of HNE on reactive oxygen species (ROS) production and on protein kinase C (PKC). Increased levels of HNE with decreasing PKC activity suggest PKC is a target for HNE adductation prior to oxidative burst. Additionally, localization of PKC to the cell membrane was prevented with the introduction of HNE, demonstrating a consequence of HNE adductation on NADPH activation. The impairment of ROS by HNE suggests HNE has a greater role in foam cell formation and tissue damage than is already known. Although work has been performed to understand the effect of HNE's regulation of specific signaling pathways, details regarding its involvement in cellular metabolism as a whole are generally unknown. This study examines the impact of HNE on macrophage oxidative burst and identifies PKC as a key protein for HNE suppression and eventual metabolic response.

Keywords

Oxidative burst; 4-hydroxynonenal; macrophage activation; multianalyte microphysiometry; phorbol myristate acetate

INTRODUCTION

4-hydroxynonenal (HNE) is an α,β-unsaturated aldehyde that is emerging as a biochemical marker of oxidative stress in many diseases such as Parkinson's disease, Alzheimer's disease, atherosclerosis, malaria and even obesity.[1-6]

[*]**Corresponding authors**: David Cliffel: Fax: 615034301234; Tel: 615032202861; d.cliffel@vanderbilt.edu. David Wright: Tel: 615032205516; david.wright@vanderbilt.edu. .

Author Contributions The manuscript was written through contributions of all authors. All authors have given approval to the final version of the manuscript.

ASSOCIATED CONTENT Supporting Information Available. Conversion of Raw MMP Measurements to Metabolic Rate Values (Figure S-1). HNE effects on macrophage metabolism as a function of concentration and exposure time (Table S-1). PMA-induced macrophage oxidative burst as a function of HNE pre-exposure at varying concentrations and time (Table S-2). This material is available free of charge via the Internet at http://pubs.acs.org.

During cellular oxidative stress, HNE is formed by means of membrane lipid peroxidation initiated by reactive oxygen species.[7] HNE is a highly reactive electrophile that covalently modifies DNA and protein, resulting in genetic mutations, altered cellular function and ultimately concentration-dependent cell death.[8-10]

HNE is formed as a secondary oxidation product of the peroxidation of cellular membrane-rich fatty acids, including arachidonic and linoleic acids. The primary reactants for HNE include the amino acid residues of cysteine, histidine and lysine and typically occur due to the formation of Michael adducts and/or Schiff bases. HNE modification of cellular proteins and enzymes results in a wide range of cellular dysfunction, including protein and nucleic acid synthesis and mitochondrial and cellular respiration, as well as specialized cell functions such as oxidative burst in monocytes.[11-13]

In the case of specialized cell function, professional phagocytes such as macrophages engulf microbial intruders and effectively kill and eradicate the foreign bodies. During this process, NADPH oxidase (nicotinamide adenine dinucleotide phosphate-oxidase) translocates to the phagolysosome to provide the antimicrobial superoxide (O^{-}_{2}) substrate for reactive oxygen and nitrogen species (ROS, RNS).[14] These species are primary indicators of oxidative stress and can lead to lipid modifications affecting cellular metabolism as a whole.[15-17] Exogenous HNE exposure has been shown to dramatically impair macrophage response to pathogenic organisms, including inducible nitric oxide synthase (iNOS), phorbol ester stimulated oxidative burst, and phagocytosis.[12, 18] In order to understand the metabolic processes occurring in cells in response to stimuli, measurements must be dynamic, rather than traditional endpoint assays.[19] Measurements taken in real-time will determine immediate fluxuations in extracellular metabolites that occur in response to activating agents, as opposed to gene expression. An excellent test case for the relevance of such measurements is to examine the phorbol ester activation of NADPH oxidase and the subsequent production of ROS in macrophage like cells.[20-22]

A study of the dynamic effects of HNE and phorbol myristate acetate (PMA) on macrophage-like RAW 264.7 cells was conducted to examine the cellular processes involved in oxidative burst.[23] Dynamic measurements were achieved using a multianalyte microphysiometer (MAMP) that simultaneously measures multiple extracellular analytes involved in metabolism in real-time.[24] Measuring the response of multiple cells normalizes cellular variability and local fluctuations, improving the study of complete cellular dynamics measured over time.[15, 25] The MAMP is based on a core cell-based assay platform known as the Cytosensor microphysiometer, which originally measured only extracellular acidification rates (ECARs) in cultured cells.[24, 26-31] Measurement of cellular oxygen consumption (aerobic) and lactate production (anaerobic) in concert allows for metabolic changes to be quantitatively assessed for each independent energy pathway. By integrating both an oxygen sensor and a lactate sensor with the acidification sensor, a more complete metabolic profile of energy metabolism can be achieved.[24] Monitoring multiple analytes simultaneously provides a more integrative approach into the complexity of macrophage metabolism.[32]

This study is directed at understanding the metabolic changes induced on macrophages upon exposure to HNE. Multianalyte microphysiometry was used to monitor real-time perturbations in acidification rate, lactate production and oxygen consumption. RAW 264.7 murine macrophages were exposed to increasing concentrations of HNE at various time intervals to assess both concentration and temporal dependence of HNE toxicity and immunosuppression, therefore evaluating both aspects simultaneously.[9] Following online HNE treatment, macrophage cells were activated with PMA to measure the corresponding change in metabolism upon initiation of oxidative burst. This study shows that HNE is a potent modulator of cellular metabolism that readily inhibits PMA-induced oxidative burst

in macrophages. Additional experiments examine the complex nature of HNE toxicity on macrophage function, covalent modifications of downstream signaling proteins such as protein kinase C (PKC) and the resulting suppression of oxidative burst and NADPH oxidase activity.

EXPERIMENTAL PROCEDURES

Materials

Glucose oxidase (GOx, *aspergillus niger*), lactate oxidase (LOx, pediococcus), bovine serum albumin (BSA, Fraction V, 96%), glutaraldehyde (25% solution in water), and 3-aminophthalhydrazine (luminol) were purchased from Sigma Aldrich (St. Louis, MO). RPMI 1640 low-buffered medium and all Cytosensor consumable materials were obtained from Molecular Devices (Sunnyvale, CA). Nafion (perfluorosulfonic acid-PTFE copolymer, 5% w/w solution) and platinum wire (0.13 mm, 0.5 mm and 1.5 mm) were obtained from Alpha Aesar. HNE, PMA, and the polyclonal anti-PKC antibodies were obtained from Calbiochem. Fetal bovine serum was purchased from Atlanta Biologicals. Penicillin/streptomycin was purchased from Mediatech. The mouse macrophage cell line, RAW 264.7, was obtained from the American Type Culture Collection.

Multianalyte Microphysiometer Enzyme-based Electrodes

Cytosensor microphysiometer plunger heads were purchased from Molecular Devices, Inc. and modified for multianalyte measurement by constructing multiple platinum electrodes at the face of the plunger head as described previously.[24] Platinum wires were inserted into predrilled holes through the plunger head and sealed with a non-conductive white epoxy, polished with emery paper using a customized brass jig, and further polished with 1 μm diamond paste until flush with the plunger head surface. The enzyme film solutions consisted of 5 mg GOx and 0.1 mg LOx dissolved in a 10% BSA/PBS solution and were cross-linked with either 5 μL or 1 μL of 25% glutaraldehyde solution, respectively. Each enzyme film solution was prepared fresh and a minimal amount applied to the platinum electrode. Enzyme films were allowed to dry for 30 minutes, and prior to use GOx and oxygen electrodes were coated with a minimal amount of 5% Nafion (w/w).

Glucose measurements were obtained during each experiment but were excluded from the results analysis due to the lack of appreciable signal change throughout the study. Both GOx and LOx convert their respective substrate to hydrogen peroxide, which is then detected amperometrically by applying a +0.6 V potential to oxidize two hydrogen peroxide molecules to water and oxygen at a platinum electrode. The immobilized enzymes directly transfer electrons to the platinum electrodes measuring the local concentration of the reaction products.[33, 34] Changes in oxygen consumption were measured amperometrically (−0.45 V) and all electrode potentials were set versus a Ag/AgCl reference electrode. Acidification rates were measured by traditional operation of the Cytosensor instrument as specified by the manufacturer. Control experiments were performed to ensure no direct effect of HNE on the sensors.

Cell Culture

The adherent mouse macrophage cell line, RAW 264.7, was maintained in continuous culture with RPMI 1640 medium, supplemented with 10% (v/v) fetal bovine serum and 100 U/mL penicillin/streptomycin in a 5% CO_2, 37 °C atmosphere.

MAMP Instrument Operation

The MAMP was operated under standard Cytosensor microphysiometer conditions utilizing a 60-s flow cycle and a 60-s stop-flow cycle. Prior to insertion of the modified plunger head,

the MAMP was conditioned by flowing low-buffered RPMI 1640 modified media through the system for 30 minutes. This low-buffered media lacks FBS and other proteins present in the culture media that might interfere with experimental aims. Sensor chambers and Teflon debubblers were preheated for 30 minutes in order to ensure an optimum temperature (37 °C) for data collection. After complete conditioning, the modified sensor head was placed in the sensor chamber and cells (plated 4 hours prior to the experiment at 3×10^5 RAW 264.7 cells/capsule cup) were allowed to equilibrate for 20 minutes.

MAMP Metabolic Data Collection and Interpretation

Electrochemical measurements were allowed to run for 50 minutes prior to the addition of HNE (0-300 μM) and/or PMA (16 μM) in the running medium. For measurements of the time-dependent and concentration-dependent effects of HNE, the following time course was performed for each experiment: (A) 60 minute equilibration period (Media); (B) 0, 20, 40 or 60 minute HNE exposure (0, 50, 100, 200 or 300 μM); (C) 30 minute stabilization period. Oxidative burst measurements consisted of: (A) 60 minute equilibration period (Media); (B) 10 minute 16 μM PMA exposure. To determine the effects of HNE on PMA-induced oxidative burst, the following time course was performed for each experiment: (A) 60 minute equilibration period (Media); (B) 0, 20, 40 or 60 minute HNE exposure (0, 50, 100, 200 or 300 μM HNE in media); (D) 30 minute equilibration period; (E) 10 minute 16 μM PMA exposure; (F) 50 minute equilibration period. Data points were collected in real-time and extracted from stop-flow measurements at 2-minute intervals (2 min = 1 cycle).

The ECAR data were recorded in normal operating order by the Cytosensor microphysiometer. Electrochemical measurements for lactate and oxygen were collected on either a CHI 1030 multipotentiostat (CH Instruments, Austin, TX) or an in-house custom quad-multiplexed multipotentiostat.[35] ECAR data were plotted as -μV/s versus time (s). The changes in lactate production rate (LPR) and oxygen consumption rate (OCR) were quantified by calculating the change in signal (nA) during stop-flow events.[36] Each cycle measurement was plotted as signal increase/decrease (nA) versus time (2 min). Baseline correction for all measurements was performed by linear-fit correction from the linear extension of the initial equilibration period. The linearized metabolic curves were normalized to 1 with experimental changes represented by percent of control. Overall relative changes in metabolism were presented as the average percentage value of 10 cycles upon introduction of fresh medium.

Luminescence Measurements of Inhibition of RAW 264.7 ROS Production with HNE

RAW 264.7 cells were plated overnight in 6 well plates at a density of 4×10^6 cells per well. The cells were washed once with sterile PBS followed by incubation with HNE (0-50 μM) for 3 hours. After HNE treatment, the cells were washed once with cold PBS and treated with 100 nM PMA in PBS for 5 minutes to initiate oxidative burst. After 5 minutes, the supernatant was removed and transferred to luminometer cuvettes. Upon addition of 50 μL of 1.0 mM luminol, luminescence was measured for 10 seconds using a Moonlight 3010 luminometer to determine the extracellular ROS.

Western Blot Analysis of HNE treated Cell Lysates

RAW 264.7 mouse macrophage cells were plated overnight at a density of 4×10^6 cells per 100 mm dish. The following day, the cells were treated with 10 mL of 35 μM HNE prepared in media and incubated at 37 °C, 95% humidity and 5% CO_2. - Once the allotted time (0, 0.5, 1.0, 1.5, 2.0, 2.5 and 3.0 hours) had passed, the samples were removed from the incubator, washed 3 times with cold PBS and treated with 400 μL of cold lysis buffer (25 mM Tris-HCl, pH 7.4, 0.25 mM sucrose, 2.5 mM EDTA, 2.5 mM DTT). After 5 minutes of rapid agitation, the samples were scrapped, pipetted to microcentrifuge tubes, and gently

sonicated with a probe sonicator. Next, the samples were centrifuged for 45 minutes at 16,100 gs.

The samples were examined by gel electrophoresis/Western blotting at a 2 μg/μL concentration and run on Novex 10% Tris-glycine gels (Invitrogen) followed by transfer to polyvinylidene difluoride membranes (Invitrogen). After complete transfer, the membranes were blocked for 1 hour or overnight with 5% nonfat dry milk dissolved in Tris-Tween buffer (TBST) composed of 25 mM Tris-HCl, pH 7.4, with 137 mM NaCl, 2.7 mM KCl, and 0.01% Tween 20, TBST. PKC obtained from the cells was detected by incubation with rabbit polyclonal anti-PKC (α/β) (371-388) antibodies (diluted 1:230 in 5% nonfat dry milk) for 2 hours at room temperature. Standard PKC βII was detected by incubation with rabbit polyclonal anti-PKC βII primary antibody (diluted 1:100 in 5% nonfat dry milk) for 2 hours at room temperature. For both, incubation with the primary was followed by TBST washing and incubation with a horseradish peroxidase-conjugated goat anti-rabbit secondary antibody (diluted 1:2000 in 5% nonfat dry milk) for 1 hour at room temperature. HNE adducted proteins were detected by incubation with mouse monoclonal anti-HNE primary antibody (diluted 1:500 in 5% nonfat dry milk) for 2 hours at room temperature, followed by incubation with a horseradish peroxidase-conjugated goat anti-mouse secondary antibody (diluted 1:2000 in 5% nonfat dry milk) for 1 hour at room temperature. Some would choose to demonstrate the modification of protein bands by first immune precipitating 4-HNE modified protein kinase C before western blotting. This study alternatively choose to label, image, strip the antibody label and then re-label the bands thus confirming that bands labeled as PKC are indeed PKC and whether or not they were modified by HNE. This was according to Abcam® western blot protocols. An enhanced chemiluminescence Western blotting analysis detection system (Amersham Biosciences) was used to visualize the bands in all cases.

Cell treatment with HNE for confocal microscopy

For all samples, RAW 264.7 mouse macrophage cells were plated overnight at a density of 5E4 cells per Mat-tek dish. The following day, HNE-treated samples were treated with 100 μL of 35 μM HNE prepared in media and incubated at 37 °C, 95% humidity and 5% CO_2 for three hours. The samples were then removed from the incubator and washed 3 times with PBS. The HNE-treated samples and PMA-activated samples were then treated with 100 μL of 100 nM PMA. After 30 seconds, the samples were quickly washed three times with PBS. All samples (HNE-treated, PMA-activated and untreated) were then fixed by incubating the sample with 3.7% paraformaldehyde for ten minutes at 37 °C, 95% humidity and 5% CO_2 for ten minutes. The samples were then again rinsed twice with PBS. All samples were then permiablized by treating with 0.2% Triton X-100 for ten minutes at room temperature. After rinsing the samples with PBS three times, 2% BSA was added to the samples for 1 hour at 4 °C to block for subsequent labeling. The cells were then labeled using anti-PKC primary antibodies (1:500 dilution), followed by 10 nM 525 quantum dot conjugated goat anti-mouse secondary antibodies. Samples were finally washed twice with PBS, covered with 2 mL of fresh PBS and immediately imaged on the Zeiss LSM 510 Meta inverted confocal microscope. Fluorescence imaging of PKC was accomplished by excitation at 488 nm, followed by collection using a long-pass filter 505 nm.

RESULTS AND DISCUSSION

Metabolic Impact of HNE on Steady State Macrophage Metabolism

To explore the impact HNE imposes on energy metabolism, RAW 264.7 murine macrophages were subjected to HNE exposure at varying concentrations and for increasing times. The solutions of HNE were made up immediately prior to the experiments and

therefore the extracellular concentrations of HNE are known by constantly perfusing fresh solutions of HNE. However, the authors do admit that the intracellular concentrations are not known. This would make an intriguing future study: testing the waste media for HNE content in line with the microfluidic device. This would allow assessment of the amount of HNE which perfused into the cell. For these studies, the concentration of HNE replenished extracellularly is reported. Changes in the levels of extracellular analyte were determined by converting the raw data into metabolic rate values by calculating the change in signal that occurred during stop-flow periods. The data were normalized by setting the initial rates measured during the equilibrium period to one. Since there is variation among runs where initial activity levels are dependent on cell activity and specific concentration, the experiments needed to be normalized in order to compare net metabolic effect. Raw data prior to being normalized (example normalization: Figure S-1) is nearly impossible to directly compare. The final change in rate was determined by averaging the last five measurements post-exposure. This allowed comparison of net change across multiple HNE doses and exposures. The experimental results show that macrophage oxidative burst is disrupted by HNE exposure in both a concentration- and time-dependent manner (Figure 1, Table S-1). The reproducibility of all experiments is noted by the standard deviations reported in tables S-1 and S-2.

Addition of HNE resulted in a dose-dependent reduction in extracellular acidification at all concentrations. At the highest concentration (300 μM) and longest exposure (60 min), the steady state macrophage ECAR dropped to 22 ± 3% of baseline.

In terms of anaerobic metabolism, LPR experienced a similar dose-dependent response in terms of both concentration as well as exposure. As with ECAR metabolism, LPR followed a concentration-dependent reduction to 11 ± 6% of baseline after 60 minutes of exposure at the highest concentrations (300 μM). The changes in LPR suggest that lactate response is slightly more sensitive to HNE in a concentration-dependent manner.

On the contrary, OCR proved to be much more resilient to HNE toxicity as a whole. At HNE concentrations of 0-200 μM, oxygen consumption remained stable at >80% OCR with very little discrimination between exposure times. Cell viability was confirmed after each experiment by carefully removing the polycarbonate membrane and staining with trypan-blue using a standard microscope. Cell death was ascertained when visual inspection determined that greater than 95% of the cell culture was stained with trypan blue. At the highest concentration (300 μM), a dramatic drop in OCR was observed for each treatment in a time-dependent manner. Macrophage oxygen consumption was essentially attenuated to 12.7 ±6% after 60 minutes of exposure to 300 μM HNE and is indicative of cell death. This same conclusion can be made for both LPR and ECAR at high concentration and exposure. Cell death was confirmed after 60 minutes of exposure to 300 μM HNE using trypan-blue staining.

Overall, the metabolic rate data suggest that RAW 264.7 macrophages are susceptible to HNE toxicity at an effective dose as low as 0.12 nmol HNE/10^5 cells (50 μM, 2.8 μL chamber volume). During each 60 second flow period, the cells are constantly perfused with a solution of HNE, resulting in total chamber volume renewal of nine times a minute. In traditional well plate assays, no renewal occurs, and extracellular HNE concentration decreases with time as intracellular HNE concentration increases. Constant perfusion of HNE in the cytosensor kept the extracellular environment uniform over time allowing changes in metabolic rates to be seen at lower concentrations and on the same time scale as the biological events of interest.

Metabolic Rate Profile of PMA-induced Oxidative Burst in RAW 264.7 Macrophages

To examine the energy metabolism of oxidative burst during macrophage activation, RAW 264.7 cells were treated for 10 minutes (5 cycles) with 16 μM PMA and metabolic changes were monitored thereafter for 30 minutes (Figure 2A). Immediately following PMA exposure, a dynamic change for each metabolic rate was calculated. This was repeated (n=4) and the metabolic rates were averaged, yielding lactate production exhibiting the largest increase (30 ± 10%) followed by ECAR (26 ± 9%) and OCR (16 ± 11%) (Figure 2B). The overall increase in metabolic activity is consistent with the enzymatic activation of NADPH oxidase.

PMA activation of RAW 264.7 cells displayed a gradual but pronounced increase in LPR immediately upon exposure. When PMA was removed from the medium, LPR was sustained at an elevated rate constant for greater than 2 hours. The increased LPR is directly related to an increase in anaerobic respiration. Unlike the gradual increase observed for LPR, the OCR displayed a more pronounced temporal increase, reaching a maximum OCR after 50 minutes post PMA treatment. In the case of oxygen consumption, an increase in OCR would be expected due to NADPH oxidase conversion of extracellular molecular oxygen to superoxide and a PMA-induced oxidative burst of RAW 264.7 cells. Furthermore, the cells displayed a sharp increase in acidification rate initially (t=0-10 min) that peaked after PMA was removed from the running media. A gradual decrease in ECAR was observed for the remainder of the experiment but remained elevated above baseline after 2 hours. This data correlates well with published literature as maximal ROS production upon activation with PMA occurs after 3-7 minutes and PKC localization in response to PMA occurs within 5 minutes.[19, 37] PMA is a small organic molecule that mimics intracellular diacylglycerol and acts through activation of PKC.[38] PKC is serine/threonine kinase implicated in a number of key cellular signaling processes, such as p47phox phosphorylation.[39, 40] PMA initiation of oxidative burst begins with activation of PKC which mediates membrane assembly of multicomponent NADPH oxidase.[39] The complex biochemical interactions that occur between cellular macromolecules, such as these, and HNE result in a variety of cellular perturbations, including disruption of cytoskeletal integrity, impairment of mitochondrial respiration, inhibition of DNA, RNA and protein synthesis, as well as impairment of specialized cellular functions such as oxidative burst in professional phagocytes.[12, 18, 41] It is also thought that HNE is linked to foam cell formation and the development of atherosclerosis. [42] Inhibiting PKC would disrupt the formation of NADPH oxidase and slow down formation of ROS. This would leave only this long-living, in comparison, reactive aldehyde to mediate the inflammatory response and foam cell formation.[43, 44] Furthermore, HNE has been shown to inhibit NF-κB activation which increases tissue damage. [45, 46] Prevention of the assembly of NADPH through adduction to PKC would therefore increases the amount of damage to the cell, more than what would be achieved through adduction to NF-κB alone. [47]

Collectively, these results paint a detailed metabolic picture of macrophage cellular respiration upon activation of NADPH oxidase by PMA. Immediately following PMA introduction, macrophage ECAR, LPR and OCR rapidly increase due to increased demand for requisite cellular energy (ATP) and molecular oxygen. Following removal of PMA from the running media, a pronounced initial decline in ECAR was observed, most likely due to the ubiquitination and degradation of PKC which is followed by down regulation of NADPH oxidase.[37] In regards to energy metabolism, removal of PMA from the medium stabilizes elevated OCR and LPR but without an appreciable decline (>2hr). The primed macrophage appears to retain an elevated state of cellular respiration.

Metabolic Impact of HNE exposure on PMA-induced RAW 264.7 Oxidative Burst

The mode by which HNE inhibition of oxidative burst occurs lies within the complex protein network involved in NADPH oxidase assembly and activation. To investigate HNE inhibition of PMA-induced oxidative burst in macrophages, RAW 264.7 cells were treated with HNE (0-300 μM) at variable exposure times (0-60 min) followed by PMA activation. Metabolic rate changes were determined immediately following PMA exposure as an average of five sequential data points, and are presented as percent to normalized baseline.

While MAMP measurements do not directly measure NADPH oxidase generation of superoxide, the metabolic changes that are elicited by PMA activation provide a unique metabolic fingerprint for comparison against HNE-treated samples. Pretreatment of RAW 264.7 cells with HNE suppresses PMA-induced metabolic changes to some degree and induces a negative response for each metabolite at high concentration and exposure time (Figure 3, Table S-2). Looking first at metabolic rates at low HNE concentrations (50 and 100 μM), metabolic measurements revealed only minor changes in metabolic response with respect to HNE pretreatment. For cells exposed to 100 μM HNE, PMA stimulation immediately increased ECAR at a 2-fold higher ECAR as compared to control. At higher HNE concentrations (200 and 300 μM), ECAR starts to drop off and terminate with negative ECAR changes. For LPR changes, a steep regression into negative LPR begins at the 100 μM - 60 minute data point and terminates at 300 μM – 60 minutes with a 50% reduction in lactate signal. At these concentrations, PMA treatment at 16 μM for 5 cycles (8 nmols) severely attenuates anaerobic metabolism. The corresponding OCR for high HNE concentrations remains relatively stable without any distinguishable fluctuations, excluding the 300 μM - 40 minute and 300 μM - 60 minute time points.

Collectively, the results of MAMP PMA-stimulation measurements show that typical metabolic increases upon PMA activation of NADPH oxidase are severely impaired at concentrations greater than 200 μM HNE and issue a negative metabolic effect at high concentrations. While the effects of HNE on steady state macrophage metabolism occurs in a concentration- and time-dependent manner, changes in PMA-activation metabolism were not consistent with respect to cellular metabolism as a whole. This leads one to believe that inhibition of oxidative burst by HNE is not simply inactivation of the superoxide generating enzyme, but the result of changes in downfield intracellular signaling pathways which can lead to incomplete assembly.

HNE Inhibition of Oxidative Burst in RAW 264.7 Cells Assessed by Luminol

HNE exhibited a concentration-dependent inhibition of ROS with an EC_{50} value of 18.4 ± 1.2 μM, which translates to an effective dose of 0.69 ± 0.05 nmol HNE/10^5 cells. (Figure 4A). This value is consistent with previously published values for murine macrophages which reported an EC_{50} value of 27 μM.[48] To examine the temporal effects of HNE on PMA-induced ROS generation, RAW 264.7 cells were treated with 35 μM HNE (1.33 nmol HNE/10^5 cells) for 0-3 hours and subsequently activated with 16 μM PMA to determine the change in ROS generation. The results indicate a time-dependent inhibition of macrophage oxidative burst with a 50% reduction of ROS generation after 1 hour (Figure 4B). ROS generation was further reduced to 20% following 2 hours of exposure and completely attenuated after 3 hours. Clearly, HNE has a strong inhibitory effect on macrophage ROS generation depending on both concentration and exposure time.

It is difficult to compare the results of HNE inhibition of PMA induced oxidative burst measured in the mycrophysiometer with those assessed through luminescence. The volume of media HNE was introduced into, number of exposed cells and mode of exposure were very different for these two experimental conditions: static versus perfusion. It is important

to consider how the cells are affected in each of these very unique conditions. Some might wonder why we looked at 50-300 μM concentration in the MAMP and then 5-50 μM using chemiluminescence, therefore wondering if 300 μM HNE is too high of a concentration to dose the cells. To explain this fuller, the volume above the cells, whether or not diffusion is the dominant type of mass transport, and if the flow of HNE is static or dynamic all must be considered. Most literature examples explore HNE modifications in the lower μM range, but all of these were static experiments.[45, 46] Within the mycrophysiometer, the sensor covers 30% of the cells in a chamber volume of 2.8 μL.[26] The cells in the well plates were exposed to a volume of 3 mL. After normalizing the experiments to moles of HNE/10^5 cells, the effective dose of HNE used in each experiment can be compared. However, it is not possible to directly compare the exposure times as microfluidic measurements expose the cells to more unique molecules than in a system where the concentration is not continually refreshed. In the luminescence study, the cells were exposed to 5-50 μM (0.19-1.88 nmol HNE/10^5 cells) for 3 hours, while cells in the mycrophysiometer were exposed to a non-lethal range of 50-200 μM (0.12-0.49 nmol HNE/10^5 cells) for 20-60 minutes and 300 μM (0.74 nmol HNE/10^5 cells) for 20-40 minutes. While 300 μM appeared to be too high at first, it actually had a lower effective does than the static experiments and therefore needed to be tested. While it may appear that the cells in the well plate are receiving a larger total amount of HNE, the constant perfusion of HNE to the microphysiometer chamber increases the effective dose. HNE readily diffuses through the cell membrane, and constant replacement of extracellular HNE allows for the possibility of a greater increase in intracellular HNE. Both the static and perfusion studies could be used to draw the same conclusion: HNE demonstrates its effects in a concentration- and time-dependent manner.

Formation of HNE Adducts to PKC

The potent ability of HNE to inhibit ROS generation and to affect metabolic rates in a dose- and time-dependent manner suggests that HNE could have adverse consequences on multiple proteins in the NADPH oxidase signalling pathway. To investigate the inactivation of NADPH oxidase, we explored the ability of HNE to chemically modify PKC, a protein vital in the assembly of NADPH oxidasel.[40]

Inhibition of PKC activity has been shown to occur with HNE levels as low as 10 μM.[49] Once activated, PKC functions by phosphorylating a number of downstream substrate proteins that regulate multiple cellular processes, including oxidative burst.[40] Of the eleven known isoforms of PKC, the βII isoform has been implicated in the phosphorylation of p47 phox which ultimately results in the translocation of the cytosolic components of NADPH oxidase to the cellular membrane. Therefore, inhibition of PKC would prevent the assembly of NADPH oxidase. Since HNE readily forms covalent protein modifications, it is plausible that the observed oxidative burst inhibition is due to formation of HNE adducts on key amino acid residues of PKC. While PKC is not the only possible target to be affected by HNE adduction in a cell, and this simply adds to the summative response described earlier, the connection between increased levels of HNE and decreased PKC activity provides an intriguing connection between the observed microphysiometery results and possible adduct formation.

To examine the possibility of HNE adduct formation on intracellular PKC, RAW 264.7 cell lysates were isolated from samples treated in a time-dependent manner (0-3 hr) with 35 μM HNE and examined for the presence of HNE adducts on PKC by Western blot analysis. A reproducible PKC-labeled band for each time point suggests that cellular integrity remained consistent from 0-3 hours (Figure 5A). After the initial 0 hour time point, HNE-adduct formation became increasingly prominent as a function of exposure time (Figure 5B). HNE treatment does not induce expression of PKC. Rather, modification appears to be time-dependent where increased amounts of PKC are targeted by HNE with increased time.

Figure 5B demonstrates the increase in HNE-modified PKC, not an increase in expression. The temporal component associated with HNE protein adduction has also been documented for other proteins, such as myoglobin, which indicated that sterically available basic amino acid residues were requisite for HNE-protein adduct formation. This study identifies PKC as a key protein for HNE suppression and eventual metabolic response. HNE is promiscuous and adducts strongly with many proteins, binding cysteine, histidine, and lysine. It is rare to know the exact mechanism of HNE modification of any protein and the specific binding sites and metabolites bound are outside the scope of this study. It has been shown in previous studies, however, that the accessibility of the active site to the solvent yields a higher percentage of HNE modifications. It has been shown in other studies that true targets have been identified on the basis of whether or not HNE binds in a concentration dependent manner.[50] Since the effects of HNE on PKC were shown to occur in a concentration- and time-dependent manner, it demonstrates that PKC is a true target of HNE. Therefore, the binding which occurs would be between HNE and PKC. This was further shown using monoclonal anti-HNE antibodies which identified HNE adducted to PKC within a western blot (Figure 5B).

A critical step in proper PKC activation is the translocation of the protein from the cytosol to the membrane, followed by its partial insertion into the plasma membrane. The effect of HNE adduct formation on PKC translocation was examined by confocal microscopy. Anti-PKC antibodies were used to image the subcellular location of the protein prior to and following activation with PMA. Cells which had previously been treated with HNE were similarly labeled. Untreated cells demonstrated proper translocation of PKC from the cytosol to the plasma membrane in as little as 30 seconds after PMA activation (Figure 6). This migration from a cytosolic distribution to plasma localization is consistent with what has previously been published in the literature. Confocal microscopy has been used to demonstrate translocation of several different PKC isoforms in response to phorbol activation in both live and fixed cells.[37, 51] In contrast, samples previously treated with HNE did not show translocation upon PMA activation, but rather remain diffused throughout the cytosol. This provides evidence that the adduction of HNE to PKC has serious deleterious consequences on the protein function, and subsequent NADPH activation. The propensity of HNE to form intracellular protein adducts with PKC in a temporal and concentration-dependent manner highlights the complex experimental approach needed to identify the key proteins, enzymes and other cellular signaling molecules involved in HNE impairment of macrophage oxidative burst. The rate of metabolism depends on the individual rates of adduction and detoxification, which can vary drastically by cell type. [52] The authors are unaware of articles presenting the metabolic rate of HNE in macrophages, the rates of other cells, such as Kupffer cells, has been studied. [52] While you could average the rates of multiple cells, the exact rate could never be more than simply an average of multiple reaction rates (Michael additions, Schiff base adducts, etc) and diffusion constants, all of which have a high biological variance. [44, 47] Furthermore, the accessibility of each adduct site can slow down the metabolism of HNE and the activation of PKC is not completely understood. [50, 52] This study demonstrates the adduction of HNE to PKC and does not seek to establish the rate of this reaction.

CONCLUSIONS

The main mode of cellular HNE toxicity results from covalent adduction and modification of susceptible proteins and enzymes.[17, 53] Cellular exposure to HNE produced a dose- and time-dependent reduction of metabolic rate in comparison to control experiments. RAW 264.7 cells treated with HNE prior to PMA activation exhibited a reduction in the expected metabolic flux at low concentrations/exposure (0-100 μM) and were completely attenuated or cytotoxic at high concentrations/exposure of HNE (200-300 μM). Luminol-based studies

of PMA-treated cells showed a dose- and time-dependent inhibition of ROS production. The temporal effects associated with metabolite measurements and luminol experiments suggest that other requisite signaling proteins/enzymes are involved in oxidative burst inhibition. Western blot analysis of PKC from RAW 264.7 cell lysates exposed to 35 μM HNE displayed a time-dependent sensitivity to HNE adduct formation identifying PKC as a target for HNE adduction. This leads to speculation as to the exact nature of HNE toxicity. In order to understand the dynamics of HNE inhibition of oxidative burst, further analysis of HNE interaction with other proteins in the NADPH oxidase signaling pathway is needed.

Supplementary Material

Refer to Web version on PubMed Central for supplementary material.

Acknowledgments

We thank Eduardo Andrade Lima and Ronald Reiserer for the development of the quad-multiplexed multipotentiostat, and Allison Price and Shellie Richards for their editorial assistance.

Funding Sources The work was supported in part by Vanderbilt Institute for Integrative Biosystems Research and Education, as well as a grant from the National Institute of Allergy and Infectious Diseases (U01 AI061223).

ABBREVIATIONS

Luminol	3-aminophthalhydrazine
BSA	bovine serum albumin
ECAR	extracellular acidification rates
GOx	glucose oxidase
HNE	4-hydroxynonenal
iNOS	inducible nitric oxide synthase
LOx	lactate oxidase
LPR	lactate production rate
MAMP	multianalyte microphysiometry
OCR	oxygen consumption rate
Nafion	perfluorosulfonic acid-PTFE copolymer
PMS	phorbol myristate acetate
PKC	protein kinase C
RNS	reactive nitrogen species
ROS	reactive oxygen species
O2-	superoxide
TBST	Tris-Tween buffer

REFERENCES

(1). Grune T, Siems WG, Schonheit K, Blasig IE. Release of 4-hydroxynonenal, an aldehydic mediator of inflammation, during postischaemic reperfusion of the myocardium. Int. J. Tissue React. 1993; 15:145–150. [PubMed: 8188453]

(2). Montine TJ, Huang DY, Valentine WM, Amarnath V, Saunders A, Weisgraber KH, Graham DG, Strittmatter WJ. Crosslinking of apolipoprotein E by products of lipid peroxidation. J. Neuropath. Exp. Neur. 1996; 55:202–210. [PubMed: 8786379]

(3). Sayre LM, Zelasko DA, Harris PL, Perry G, Salomon RG, Smith MA. 4-Hydroxynonenal-derived advanced lipid peroxidation end products are increased in Alzheimer's disease. J. Neurochem. 1997; 68:2092–2097. [PubMed: 9109537]

(4). Selley ML. (E)-4-hydroxy-2-nonenal may be involved in the pathogenesis of Parkinson's disease. Free Radical Biol. Med. 1998; 25:169–174. [PubMed: 9667492]

(5). Soares AF, Guichardant M, Cozzone D, Bernoud-Hubac N, Bouzaidi-Tiali N, Lagarde M, Geloen A. Effects of oxidative stress on adiponectin secretion and lactate production in 3T3-L1 adipocytes. Free Radical Biol. Med. 2005; 38:882–889. [PubMed: 15749384]

(6). Uchida K, Toyokuni S, Nishikawa K, Kawakishi S, Oda H, Hiai H, Stadtman ER. Michael addition-type 4-hydroxy-2-nonenal adducts in modified low-density lipoproteins: markers for atherosclerosis. Biochemistry. 1994; 33:12487–12494. [PubMed: 7918471]

(7). Marnett LJ, Riggins JN, West JD. Endogenous generation of reactive oxidants and electrophiles and their reactions with DNA and protein. J. Clin. Invest. 2003; 111:583–593. [PubMed: 12618510]

(8). Hill BG, Dranka BP, Zou L, Chatham JC, Darley-Usmar VM. Importance of the bioenergetic reserve capacity in response to cardiomyocyte stress induced by 4-hydroxynonenal. Biochem. J. 2009; 424:99–107. [PubMed: 19740075]

(9). Zarkovic N. 4-hydroxynonenal as a bioactive marker of pathophysiological processes. Mol. Aspects Med. 2003; 24:281–291. [PubMed: 12893006]

(10). Uchida K. 4-Hydroxy-2-nonenal: a product and mediator of oxidative stress. Prog. Lipid Res. 2003; 42:318–343. [PubMed: 12689622]

(11). Poli G, Schaur RJ. 4-Hydroxynonenal in the pathomechanisms of oxidative stress. IUBMB Life. 2000; 50:315–321. [PubMed: 11327326]

(12). Carney CK, Schrimpe AC, Halfpenny K, Harry RS, Miller CM, Broncel M, Sewell SL, Schaff JE, Deol R, Carter MD, Wright DW. The basis of the immunomodulatory activity of malaria pigment (hemozoin). J. Biol. Inorg. Chem. 2006; 11:917–929. [PubMed: 16868743]

(13). Schwarzer E, Kuhn H, Valente E, Arese P. Malaria-parasitized erythrocytes and hemozoin nonenzymatically generate large amounts of hydroxy fatty acids that inhibit monocyte functions. Blood. 2003; 101:722–728. [PubMed: 12393662]

(14). Forman HJ, Torres M. Redox signaling in macrophages. Mol. Aspects Med. 2001; 22:189–216. [PubMed: 11679166]

(15). Amatore C, Arbault S, Chen Y, Crozatier C, Tapsoba I. Electrochemical detection in a microfluidic device of oxidative stress generated by macrophage cells. Lab Chip. 2007; 7:233–238. [PubMed: 17268626]

(16). Forman HJ, Dickinson DA, Iles KE. HNE--signaling pathways leading to its elimination. Mol. Aspects Med. 2003; 24:189–194. [PubMed: 12892996]

(17). Vila A, Tallman KA, Jacobs AT, Liebler DC, Porter NA, Marnett LJ. Identification of protein targets of 4-hydroxynonenal using click chemistry for ex vivo biotinylation of azido and alkynyl derivatives. Chem. Res. Toxicol. 2008; 21:432–444. [PubMed: 18232660]

(18). Neely MD, Amarnath V, Weitlauf C, Montine TJ. Synthesis and cellular effects of an intracellularly activated analogue of 4-hydroxynonenal. Chem. Res. Toxicol. 2002; 15:40–47. [PubMed: 11800596]

(19). Swindle EJ, Hunt JA, Coleman JW. A Comparison of Reactive Oxygen Species Generation by Rat Peritoneal Macrophages and Mast Cells Using the Highly Sensitive Real-Time Chemiluminescent Probe Pholasin: Inhibition of Antigen-Induced Mast Cell Degranulation by Macrophage-Derived Hydrogen Peroxide. J. Immunol. 2002; 169:5866–5873. [PubMed: 12421969]

(20). Pacheco-Garcia U, Legorreta-Herrera M, Hernandez-Rodriguez C, Sanchez-Garcia FJ. Multiple Mycobacterium microti derived lipids stimulate iNOS gene expression in the J774 murine macrophage cell line. Scand. J. Immunol. 2002; 56:52–58. [PubMed: 12100471]

(21). Raines KW, Kang TJ, Hibbs S, Cao G-L, Weaver J, Tsai P, Baillie L, Cross AS, Rosen GM. Importance of Nitric Oxide Synthase in the Control of Infection by Bacillus anthracis. Infect. Immun. 2006; 74:2268–2276. [PubMed: 16552057]

(22). MacMicking J, Xie Q.-w. Nathan C. Nitric Oxide and Macrophage Function. Annu. Rev. Immunol. 1997; 15:323–350. [PubMed: 9143691]

(23). Schrimpe AC, Wright DW. Differential gene expression mediated by 15-hydroxyeicosatetraenoic acid in LPS-stimulated RAW 264.7 cells. Malaria J. 2009; 8:195.

(24). Eklund SE, Taylor D, Kozlov E, Prokop A, Cliffel DE. A microphysiometer for simultaneous measurement of changes in extracellular glucose, lactate, oxygen, and acidification rate. Anal. Chem. 2004; 76:519–527. [PubMed: 14750842]

(25). Zhang X, Yin H, Cooper J, Haswell S. Characterization of cellular chemical dynamics using combined microfluidic and Raman techniques. Anal. Bioanal. Chem. 2008; 390:833–840. [PubMed: 17849101]

(26). Hafner F. Cytosensor Microphysiometer: technology and recent applications. Biosens. Bioelectron. 2000; 15:149–158. [PubMed: 11286332]

(27). McConnell HM, Owicki JC, Parce JW, Miller DL, Baxter GT, Wada HG, Pitchford S. The cytosensor microphysiometer: biological applications of silicon technology. Science. 1992; 257:1906–1912. [PubMed: 1329199]

(28). Wille K, Paige LA, Higgins AJ. Application of the Cytosensor microphysiometer to drug discovery. Recept. Channels. 2003; 9:125–131. [PubMed: 12916473]

(29). Eklund SE, Cliffel DE, Kozlov E, Prokop A, Wilkswo J, Baudenbacher F. Modification of the Cytosensor microphysiometer to simultaneously measure extracellular acidification and oxygen consuption rates. Anal. Chim. Acta. 2003; 496:93–101.

(30). Eklund SE, Snider RM, Wikswo J, Baudenbacher F, Prokop A, Cliffel DE. Multianalyte microphysiometry as a tool in metabolomics and systems biology. J. Electroanal. Chem. 2006; 587:333–339.

(31). Eklund SE, Thompson RG, Snider RM, Carney CK, Wright DW, Wikswo J, Cliffel DE. Metabolic Discrimination of Select List Agents by Monitoring Cellular Responses in a Multianalyte Microphysiometer. Sensors. 2009; 9:2117–2133. [PubMed: 22574003]

(32). Zachek MK, Park J, Takmakov P, Wightman RM, McCarty GS. Microfabricated FSCV-compatible microelectrode array for real-time monitoring of heterogeneous dopamine release. Analyst. 2010; 135:1556–1563. [PubMed: 20464031]

(33). Rhoten MC, Burgess JD, Hawkridge FM. Temperature and pH effects on cytochrome c oxidase immobilized in an electrode-supported lipid bilayer membrane. Electrochim. Acta. 2000; 45:2855–2860.

(34). Mikkelsen SR, Rechnitz GA. Conductometric tranducers for enzyme-based biosensors. Anal. Chem. 1989; 61:1737–1742. [PubMed: 2774202]

(35). Lima EA, Snider RM, Reiser RS, McKenzie JR, Eklund S, Cliffel DE, Wikswo JP. Multipotentiostat for multianalyte microphysiometry in eight electrochemical cells simultaneously. Sens. Actuators, B. (In preparation).

(36). Snider RM, McKenzie JR, Kraft L, Kozlov E, Wikswo JP, Cliffel DE. The Effects of Cholera Toxin on Cellular Energy Metabolism. Toxins. 2010; 2:632–648. [PubMed: 22069603]

(37). Köhl R, Preiss S, von Knethen A, Brüne B. Oxidized low-density lipoprotein depletes PKC alpha and attenuates reactive oxygen species formation in monocytes/macrophages. Cardiovasc. Res. 2006; 71:574–585. [PubMed: 16843450]

(38). Mosior M, Newton AC. Mechanism of interaction of protein kinase C with phorbol esters. Reversibility and nature of membrane association. J. Biol. Chem. 1995; 270:25526–25533. [PubMed: 7592722]

(39). Greene NM, Williams DS, Newton AC. Kinetics and localization of the phosphorylation of rhodopsin by protein kinase C. J. Biol. Chem. 1995; 270:6710–6717. [PubMed: 7896814]

(40). Newton AC. Protein kinase C: structure, function, and regulation. J. Biol. Chem. 1995; 270:28495–28498. [PubMed: 7499357]

(41). Schrimpe AC, Wright DW. Comparative Analysis of Gene Expression Changes Mediated by Individual Constituents of Hemozoin. Chem. Res. Toxicol. 2009; 22:433–445. [PubMed: 19191707]

(42). Borazjani A, Edelmann MJ, Hardin KL, Herring KL, Crow JA, Ross MK. Catabolism of 4-hydroxy-2-trans-nonenal by THP1 monocytes/macrophages and inactivation of carboxylesterases by this lipid electrophile. Chem.-Biol. Interact. 2011; 194:1–12. [PubMed: 21878322]

(43). Yun MR, Im DS, Lee SJ, Woo JW, Hong KW, Bae SS, Kim CD. 4-hydroxynonenal contributes to macrophage foam cell formation through increased expression of class A scavenger receptor at the level of translation. Free Radical Biol. Med. 2008; 45:177–183. [PubMed: 18456003]

(44). Alary J, Gueraud F, Cravedi J-P. Fate of 4-hydroxynonenal in vivo: disposition and metabolic pathways. Mol. Aspecs Med. 2003; 24:177–187.

(45). Ji C, Kozak KR, Marnett LJ. IκB Kinase, a Molecular Target for Inhibition by 4-Hydroxy-2-nonenal. J. Biol. Chem. 2001; 276:18223–18228. [PubMed: 11359792]

(46). Luckey SW, Taylor M, Sampey BP, Scheinman RI, Petersen DR. 4-Hydroxynonenal Decreases Interleukin-6 Expression and Protein Production in Primary Rat Kupffer Cells by Inhibiting Nuclear Factor-Î°B Activation. J. Pharmacol. Exp. Ther. 2002; 302:296–303. [PubMed: 12065730]

(47). Schopfer FJ, Cipollina C, Freeman BA. Formation and Signaling Actions of Electrophilic Lipids. Chem. Rev. (Washington, DC, U. S.). 2011; 111:5997–6021.

(48). Dianzani C, Parrini M, Ferrara C, Fantozzi R. Effect of 4-hydroxynonenal on superoxide anion production from primed human neutrophils. Cell Biochem. Funct. 1996; 14:193–200. [PubMed: 8888573]

(49). Schwarzer E, Arese P. Phagocytosis of malarial pigment hemozoin inhibits NADPH-oxidase activity in human monocyte-derived macrophages. Biochim. Biophys. Acta. 1996; 1316:169–175. [PubMed: 8781535]

(50). Fritz KS, Petersen DR. Exploring the Biology of Lipid Peroxidation-Derived Protein Carbonylation. Chem. Res. Toxicol. 2011; 24:1411–1419. [PubMed: 21812433]

(51). Majumder N, Bhattacharjee S, Bhattacharyya S, Dey R, Guha P, Pal NK, Majumdar S. Restoration of impaired free radical generation and proinflammatory cytokines by MCP-1 in mycobacterial pathogenesis. Scand. J. Immunol. 2008; 67:329–339. [PubMed: 18282229]

(52). Dubinina EE, Dadali VA. Role of 4-Hydroxy-trans-2-nonenal in Cell Functions. Biochemistry (Moscow). 2010; 75:1069–1087. [PubMed: 21077827]

(53). Li L, Hamilton RF Jr. Kirichenko A, Holian A. 4-Hydroxynonenal-induced cell death in murine alveolar macrophages. Toxicol. Appl. Pharmacol. 1996; 139:135–143. [PubMed: 8685896]

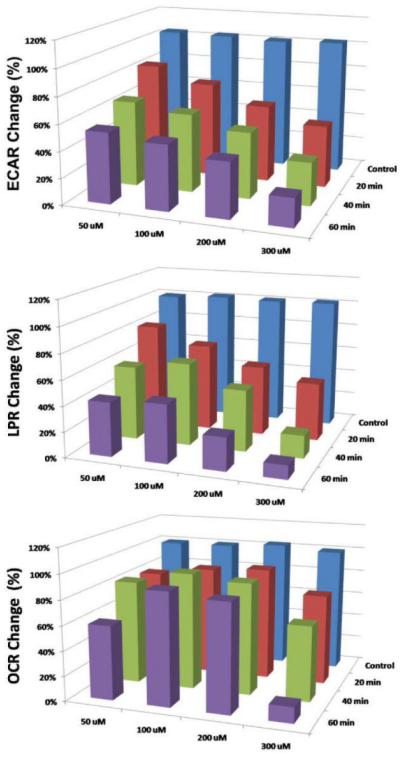

Figure 1.

3-D Composite of HNE effects on macrophage metabolism as a function of concentration and exposure time. The changes in ECAR (top), LPR (middle), and OCR (bottom) that occur as a result of HNE exposure. Control was exposed to 0 min of HNE. All other samples were exposed to HNE for the time and at the concentration noted on the axis. Rate changes are representative of final metabolic rate post-HNE exposure.

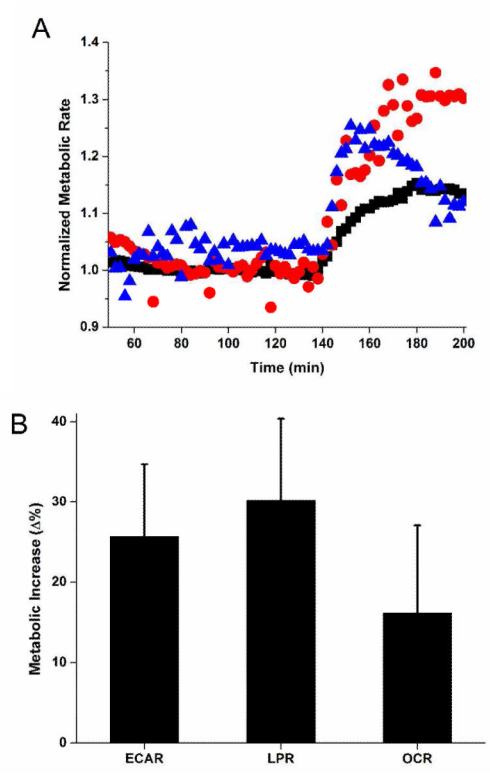

Figure 2.

PMA-stimulated macrophage metabolic response. (A) Normalized increases in ECAR (▲) LPR (■) and OCR (●) upon introduction of PMA (16 μM) at t = 140 min. (B) Average increase of each cellular metabolic rate. Determined from three independent experiments (n = 4, data shown in Table S-2).

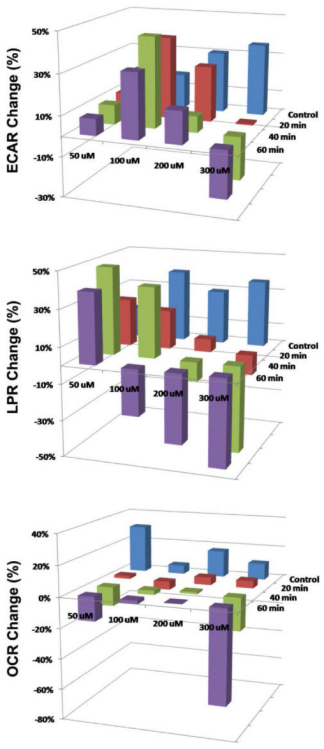

Figure 3.

3-D Composite of PMA-induced macrophage oxidative burst as a function of HNE pre-exposure at varying concentrations and time. The changes in ECAR (top), LPR (middle), and OCR (bottom) that occur as a result of PMA exposure. Control was exposed to 0 min of HNE. All other samples were pre-exposed to HNE for the time and at the concentration noted on the axis. Rate changes are representative of final metabolic rate post-PMA exposure.

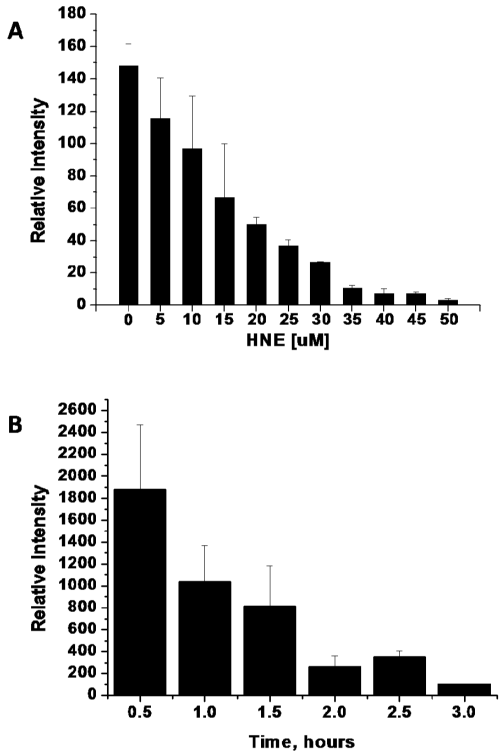

Figure 4.
HNE inhibition of PMA-induced ROS. (A) Concentration-dependent (0-50 μM HNE) and (B) Time-dependent (0-3 hr, 35 μM HNE) inhibition of ROS generation assessed by luminol enhanced chemiluminescence.

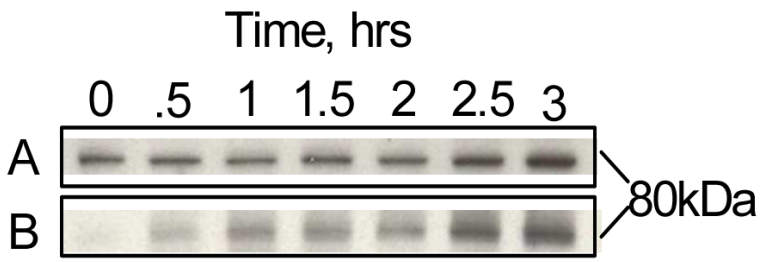

Figure 5.
Western blot analysis of HNE-modified PKC from cell lysates. (A) PKC protein bands labelled with monoclonal anti-PKC antibody and (B) 35 μM HNE-treated PKC protein bands labelled with monoclonal anti-HNE antibody.

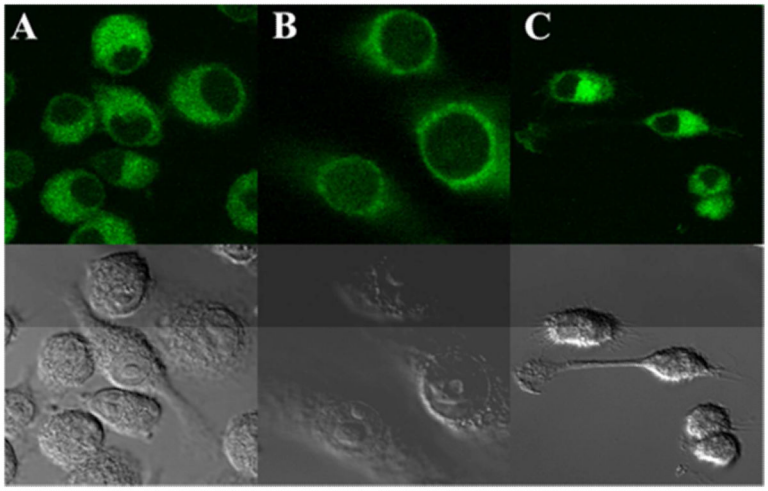

Figure 6.

Confocal microscopy of PMA and HNE treated cells. All cells were labelled with anti-PKC primary antibodies followed by 10 nM 525 quantum dot conjugated goat anti-mouse secondary antibodies. Fluorescence (top) and confocal images (bottom) of (A) untreated cells (B) cells treated with 100 μL of 100 nM PMA and (C) cells treated with 100 μL of 35 μM HNE followed by 100 nM PMA.